# The observation of the second nonet of tensor mesons with the L3 experiment

V.Schegelsky, A.Sarantsev, V.Nikonov,
A.Anisovich, M.Levtchenko

February 8, 2020

**Abstract**

The data on the reactions $\gamma\gamma \to \pi^+\pi^-\pi^0$ and $\gamma\gamma \to \mathrm{K}^0_\mathrm{S}\mathrm{K}^0_\mathrm{S}$ are collected by the L3 detector at LEP. In the reaction $\gamma\gamma \to \pi^+\pi^-\pi^0$ a strong signal consistent with the first radial excitation of the isovector tensor state, $a_2(1700)$ , is observed with the mass $M = (1722 \pm 9 \pm 8)$ MeV and the width $\Gamma = (336 \pm 20 \pm 20)$ MeV.

The mass spectrum of the $\mathrm{K}^0_\mathrm{S}\mathrm{K}^0_\mathrm{S}$ is dominated by the formation of tensor mesons. The signal at (1700-1800) MeV region is proved to be due to a new state - the tensor meson $f_2(1750)$ with mass $M = (1755 \pm 10)$ MeV and width $\Gamma = (67 \pm 12)$ MeV.

The $f_2(1750)$ state forms the second tensor nonet together with $f_2(1560)$ and $a_2(1700)$. In the $SU(3)$ based analysis the present data allows us to determine mixing angles of tensor nonets with good accuracy.

## 1 Introduction

The QCD is the theory of strong interactions and it works reliably at high energies where perturbative methods can be applied. However such approach can not be directly used at low and intermediate energies where the coupling constant is large. An important step in the development of a nonperturbative approach is an identification and classification of the strong interacting particles: hadrons. In recent years a set of experiments was carried out for search of new hadron resonances. Important discoveries have been made both in the meson and the baryon sectors, and properties of many resonances studied in details. There is no doubt that most hadron states form SU(3) multiplets manifesting their quark nature. Exotics states like glueballs, hybrid states or mesonic molecules are quite rare, if they exist at all, and usually do not show up strongly in experiments.

One of the important recent discoveries in physics of strong interactions was that meson nonets are lying on linear trajectories not only against the total spin (Regge

trajectories) but also against radial excitation number. Such a phenomenon provides a valuable information about quark interactions in the region of quark confinement; a confirmation of such behavior is one of the most important tasks for experimental physics.

Gamma-gamma collision reactions provide a powerful tool for the investigation of meson properties. It is especially valuable that the data not only supply the information about masses and widths of resonances but also about their couplings to the gamma-gamma channel which can be directly calculated in the framework of quark models. Another important feature is that meson molecules and glueball states must be produced weakly in such reactions providing a clear spectrum of quark-antiquark states.

In this paper the formation of resonances in two-photon collisions is studied via the process $e^+e^- \to e^+e^-\gamma^*\gamma^* \to e^+e^-R \to e^+e^-$ *pseudoscalar mesons*, where $\gamma^*$ is a virtual photon. The outgoing electron and positron carry nearly the full beam energy and their transverse momenta are rather small and for this reason are usually not detected. In this case the two photons are quasi-real. The cross section for this process is given by the convolution of the QED calculable luminosity function $\mathcal{L}_{\gamma\gamma}$, giving the flux of photons, with a Breit-Wigner function for a resonance. This leads to the proportionality relation between the measured cross section and the two-photon width $\Gamma_{\gamma\gamma}(R)$ of the resonance R

$$\sigma(e^+e^- \to e^+e^-R) = \mathcal{K} \cdot \Gamma_{\gamma\gamma}(R), \tag{1}$$

where the proportionality factor $\mathcal{K}$ is evaluated by a Monte Carlo integration.

The data collected with the L3 experiment during runs with Large Electron-Positron Collider(LEP-CERN) contains a lot of information on two-photon processes. The results of the Partial Wave Analysis (PWA) of two reactions - $e^+e^- \to e^+e^-\pi^+\pi^-\pi^0$ and $e^+e^- \to e^+e^-K^0_SK^0_S$ - are presented in this paper.

# 2 Event selection

The L3 experimental set up [1] is very efficient for studies of resonances produced in two-photon collisions due to L3 capability to detect low energy photons by the crystal electromagnetic spectrometer (BGO) and charged particles by the inner trackers ( silicon strips and time expansion chamber). The events are mainly accepted by the sophisticated charged particles trigger [2] ,[3].

Details of the selection procedure is described elsewhere [4]

## 2.1 The $e^+e^- \to e^+e^-\pi^+\pi^-\pi^0$ data

The $\pi^+\pi^-\pi^0$ final state is identified by :

1. Two charged tracks with a net charge of zero. The tracks must come from the interaction vertex within three standard deviations.

2. Two photon candidates, reconstructed from isolated electromagnetic showers .

3. One $\pi^0$ with a mass between 95 MeV and 155 MeV, formed by at least one photon candidate of energy greater than 80 MeVand another shower.

4. No other showers.

For a total luminosity of 663 $pb^{-1}$, 18000 events are selected.

The side bands of the $\pi^0$ mass distribution, 65-95 MeV and 155-185 MeV, used to estimate the background are shown in Fig. 1.

The $\pi^+\pi^-\pi^0$ mass distribution, where $W_{\gamma\gamma}$ is the total energy, shown in Fig. 2a, is dominated by the production of the $a_2(1320)$ state. There is a shoulder in the mass region 1.6-1.8 GeV.

The main signal in the $\pi^\pm\pi^0$ mass spectrum, presented in Fig. 2b, is due to the production of $\rho(770)$. There is very little structure in the region above 1 GeV and almost no events higher than 1.5 GeV.

The $\pi^+\pi^-$ mass distribution is shown in Fig. 2c. For $W_{\gamma\gamma}$ above 1.5 GeV the $f_2(1270)$ is present, as shown in Fig. 2d.

In all mass distributions of Fig. 2 the background, estimated from the side bands of the $\pi^0$, is indicated as a shaded histogram.

The total selection efficiency rises from a value of 0.3 % at $W_{\gamma\gamma} = 1.$GeV to 4.5 % at $W_{\gamma\gamma} = 5.0$GeV .The acceptance of the detector and the efficiency of the analysis are calculated by Monte Carlo. The efficiencies of the charged particle and higher level triggers depend on the year of data taking: they are calculated directly from the data and vary from ∼40% at low $W_{\gamma\gamma}$ to ∼90% at high $W_{\gamma\gamma}$.

## 2.2 The $e^+e^- \to e^+e^-K^0_S K^0_S$ data

The selection of KsKs events is based on the decay $K^0_S \to \pi^+\pi^-$.

The following criteria were used :

- There must be exactly four charged tracks in the tracking system with a net charge of zero; not more than 2 tracks should be within 3 standard deviation from the primary vertex.

- Events with photons are rejected. A photon is identified as an isolated shower with an energy at least 100 MeV.

The $K^0_S$ are identified by the secondary vertex reconstruction.

- The secondary vertex $\pi^+\pi^-$ mass (Fig. 3a) should be compatible with $K^0_S$ mass. The $\pi^+\pi^-$ mass resolution is $\sigma = (9.5 \pm .2)$ MeV.

- The angle $\alpha$ between the flight direction of the $K^0_S$ candidate ( taken as a line between the interaction point and the secondary vertex in the transverse plane ) and the total transverse momentum vector of the decay pions must be smaller than 0.3 rad. (Fig.3b)

- A secondary vertex should have an 'invariant' distance $d$ greater than 1.5 mm

$$d = d_0 \frac{M_{Ks}}{P_{Ks}}, \tag{2}$$

  where $d_0$ is the distance in space between the primary and secondary vertex. (Fig. 3c)

- The total transverse momentum imbalance $P_t = |\sum \vec{p}_t|$ must be smaller than 0.3 GeV. In Fig. 3d the $P_t$ distribution is compared to the Monte Carlo prediction for exclusive $K^0_S K^0_S$ formation. Some excess of the data at high values of $P_t$ might be due to inclusive $K^0_S K^0_S$ final state.

Fig. 4 shows the distribution of the mass of one $K^0_S$ candidate versus the mass of the other candidate. There is a strong enhancement corresponding to the $K^0_S K^0_S$ formation. We require that the reconstructed masses of two $K^0_S$ candidates must be inside a circle of 40 MeV radius centered on the peak of the $K^0_S K^0_S$ signal. Events inside the ring of the same surface outside of the circle might be considered as an estimate of the background in the accepted events sample.

With these selection criteria for a total luminosity of 806 $pb^{-1}$the 870 events are found. The background due to misidentified $K^0_S$ pairs is estimated to be less than 10%.

Fig. 5 shows the $K^0_S K^0_S$ mass spectrum of selected events with the mass spectrum of the background estimated as mentioned above.

# 3 Energy dependent partial wave analysis

The two-photon channel couples only to states, R , with positive C-parity. For a neutral system G-parity is determined by the isospin of R state:

$$G = Ce^{i\pi I}$$

Such constraints are unique feature of two-photon exclusive hadronic processes and very essential for efficient identification of resonances produced.

The analysis of the data is based on the method of extraction of leading singularities, suggested in Ref. [5].

The amplitude for the two-photon interaction is written as:

$$A = \sum_i \epsilon^{(1)}_\mu \epsilon^{(2)}_\nu A^i_{\mu\nu}. \tag{3}$$

Here $\varepsilon_\mu$ are the polarization vectors of the photons and the index $i$ describes three possible spin configurations, 0, 1, or 2, of the two-photon system. After averaging over the polarization of the initial photons:

$$\frac{1}{2}\sum_j \varepsilon_\mu^j \varepsilon_\nu^j = g_{\mu\nu}^{\perp\perp} = g_{\mu\nu} - \frac{P_\mu P_\nu}{P^2} - \frac{g_\mu^\perp q_\nu^\perp}{q_\perp^2} \tag{4}$$

the amplitudes corresponded to different spin combinations are orthogonal.

A system of two real photons can have either even-even or odd-odd combination of the spin and orbital momentum. One combination of the spin and orbital angular momentum operator forms $0^{++}$ state: $^{2s+1}L_J = {}^1S_0$ and $0^{-+}$ state: $^3P_0$. The $2^{++}$ partial wave can be produced from a spin 0 state with orbital momentum 2 ($^1D_2$) or from a spin 2 state with orbital momentum 0 ($^5S_2$). All other combinations are either equal to zero or reduced to one of the above combinations in the gauge invariant limit. For the $4^{++}$ state there are also two combinations: $^1G_4$ and $^5D_4$. Two combinations for $2^{-+}$ state $^3P_2$ and $^3F_2$ produce the same angular dependence in the gauge invariant limit.

From the four-vectors of each event, $j$, a likelihood function is constructed as:

$$L = \frac{1}{\sigma_{tot}} \prod_j \frac{d\sigma_j}{d\Phi} = \frac{1}{\sum\limits_n^{MC} d\sigma_n} \prod_j \frac{d\sigma_j}{d\Phi} \tag{5}$$

where $\frac{d\sigma_j}{d\Phi}$ is the calculated cross-section and $\sigma_{tot}$ is the integrated cross section over the available phase space, estimated as the sum of all the Monte Carlo events that passed the detector acceptance and the selection cuts. The parameters of the different states: the pole mass, the couplings and the width of the resonances R as well as the parameters of the polynomial background, are fitted to minimize the function $-ln\ L$.

The different final states are identified by an energy dependent partial wave analysis, which assumes the cascade decay, $\mathrm{R} \to \mathrm{R}'\pi$, and takes into account the interference between different amplitudes. The masses and widths of resonances produced in $\gamma\gamma$ channel, defined as the pole of the scattering amplitude are obtained as well as the branching ratios for decays into different $\mathrm{R}'\pi$ channels. For all found states the two-photon partial widths, $\Gamma_{\gamma\gamma}$ were calculated from the measured cross section. For $2^{++}$ resonances we also define the ratio between two photon $S$ and $D$-wave initial states.

## 3.1 The $\mathbf{e^+e^- \to e^+e^-\pi^+\pi^-\pi^0}$ reaction

Since a three pion final state has a negative G-parity only isovector $q\bar{q}$ states can be produced in the $\gamma\gamma \to \pi^+\pi^-\pi^0$ reaction. Due to conservation of $C$-parity in neutral decay modes, only $f$ $q\bar{q}$-states ($J^{PC} = 0^{++}$, $2^{++}$, $4^{++}$...) are produced in the $\pi^+\pi^-$ channel. Assuming a cascade decay, $\mathrm{R} \to \mathrm{R}'\pi$, only states R' with $J^{PC} = 1^{--}$, $3^{--}$,... are allowed in the $\pi^\pm\pi^0$ channels.

The amplitude $A^i_{\mu\nu}$, for the cascade decay $\mathrm{R} \to \mathrm{R}'\pi$ is expressed as the product of the R and R′ Breit-Wigner amplitudes with standard Blatt-Weisskopf factors $F(r,k,L)$ [6] and the angular momentum operators $O^{\alpha,i,l,j,m}_{\mu\nu}$:

$$\begin{aligned} A^i_{\mu\nu} = \sum_{\alpha l j m n k} & \frac{g^{\alpha i l}_{\gamma\gamma}\Lambda^{\alpha}_{jm}}{M^2_{\alpha n} - W^2_{\gamma\gamma} - iM_{\alpha n}\Gamma_{\alpha n}} \\ \times & \frac{O^{\alpha,i,l,j,m}_{\mu\nu}}{\sqrt{F(q,r,l)F(k^{\perp},r,m)F(k_{12},r,j)}} \\ \times & \frac{1}{M^2_{jk} - s_{12} - iM_{jk}\Gamma_j}; \end{aligned}$$

$$\begin{aligned} & P = k_1 + k_2 + k_3 \quad k^{\perp}_{\mu} = \frac{1}{2}(k_{1\mu} + k_{2\mu} - k_{3\mu} - \frac{s_{12} - m^2_{\pi}}{W^2_{\gamma\gamma}}\, P_{\mu}) \\ & k_{12\mu} = \frac{1}{2}(k_{1\mu} - k_{2\mu}) \quad P^2 = W^2_{\gamma\gamma} \quad s_{12} = (k_1 + k_2)^2 \\ & k^{\perp} = \sqrt{-k^{\perp}_{\mu}k^{\perp\mu}} \quad k_{12} = \sqrt{-k_{12\mu}k^{\mu}_{12}}\,. \end{aligned} \tag{6}$$

Here the index $\alpha$ refers to the total spin of R, the indexes $i, l$ to the spin and orbital angular momentum of the $\gamma\gamma$ system and $j, m$ to the spin of R′ and its orbital angular momentum with the spectator pion. The $M_{\alpha n}$ and $\Gamma_{\alpha n}$ are masses and total widths of resonances produced in $\gamma\gamma$ channel (index $n$ counts the number of resonances with total spin $\alpha$) while $M_{jk}$ and $\Gamma_{jk}$ denote masses and widths of $R'$ states.

The operators $O^{\alpha,i,l,j,m}_{\mu\nu}$ describe the tensor structure of the $\gamma\gamma \to \pi^+\pi^-\pi^0$ amplitude. The explicit form of these operators can be found in [7]. If resonances with same quantum numbers overlap weakly, the couplings of them with the $\gamma\gamma$ channel ($g^{\alpha i l}_{\gamma\gamma}$) are real numbers. Three body decay couplings $\Lambda^{\alpha}_{jm}$, which includes also two body coupling for the decay of R′ into two pions are complex numbers due to contributions from triangle singularities.

The total width of the resonance is defined as a sum of main decay channels of the state taken from PDG [8].

$$\begin{aligned} \Gamma = \Gamma_{tot} \sum_i Br_i \frac{\rho_i(s) k_i^{2L_i} F(r, k_{M\,i}, L_i)}{\rho_i(M^2) k_{M\,i}^{2L_i} F(r, k_i, L_i)} \\ k_{M\,i} = k_i(s{=}M^2) \qquad \rho_i(s) = \frac{k_i}{\sqrt{s}} \end{aligned} \tag{7}$$

The Blatt-Weisskopf factors were calculated with radius $r = 0.55$ fm.

## 3.2 The $\mathbf{e^+e^- \to e^+e^-K^0_S K^0_S}$ reaction

Only $J^{PC} = (2n)^{++}$, $n = 0, 1, 2, \ldots$ states decay into two neutral pseudoscalar particles. The $K_sK_s$ mass spectrum, shown in Fig. 5, is dominated by production

of tensor states. Near $K_sK_s$ threshold there is a signal from production of scalar mesons, at high masses one can see a signal from $4^{++}$ states.

Due to the spinless nature of the final state particles the amplitude structure for the decay of resonances into $K_sK_s$ is defined by orbital angular momentum operators only. These operators are constructed out of the relative momenta of kaons [9]:

$$\begin{aligned}
&0^{++} \quad {}^1S_0 \quad && X^{(0)}(k) = 1 \\
&2^{++} \quad {}^1D_2 \quad && X^{(2)}_{\mu\nu}(k) = \frac{3}{2}(k^\perp_\mu k^\perp_\nu - \frac{1}{3}k^2_\perp g^\perp_{\mu\nu}) \\
&4^{++} \quad {}^1G_4 \quad && X^{(4)}_{\mu\nu\alpha\beta}(k) = \frac{1}{8}\Big(35k^\perp_\mu k^\perp_\nu k^\perp_\alpha k^\perp_\beta \\
& && -5k^2_\perp(g^\perp_{\mu\nu}k^\perp_\alpha k^\perp_\beta + g^\perp_{\mu\alpha}k^\perp_\nu k^\perp_\beta + g^\perp_{\mu\beta}k^\perp_\nu k^\perp_\alpha \\
& && +g^\perp_{\nu\alpha}k^\perp_\mu k^\perp_\beta + g^\perp_{\nu\beta}k^\perp_\mu k^\perp_\alpha + g^\perp_{\alpha\beta}k^\perp_\mu k^\perp_\nu) \\
& && +k^4_\perp(g^\perp_{\mu\nu}g^\perp_{\alpha\beta} + g^\perp_{\mu\alpha}g^\perp_{\nu\beta} + g^\perp_{\mu\beta}g^\perp_{\nu\alpha})\Big),
\end{aligned} \tag{8}$$

where $k_1$ and $k_2$ are 4-momenta of final kaons ($P = k_1 + k_2$) and:

$$k^\perp_\mu = \frac{1}{2}g^\perp_{\mu\nu}(k_1 - k_2)_\nu \qquad\qquad g^\perp_{\mu\nu} = g_{\mu\nu} - \frac{P_\mu P_\nu}{P^2} \tag{9}$$

Defining the relative momentum as $q^\perp_\mu$ we obtain the following expressions for the $\gamma\gamma$ operators:

$$\begin{aligned}
&{}^1S_0: \quad \varepsilon^{(1)}_\mu \varepsilon^{(2)}_\nu g^\perp_{\mu\nu} \\
&{}^1D_2: \quad \varepsilon^{(1)}_\mu \varepsilon^{(2)}_\nu g^\perp_{\mu\nu} X^{(2)}_{\alpha\beta}(q^\perp) \qquad q^\perp_\mu = \frac{1}{2}g^\perp_{\mu\nu}(q_1 - q_2)_\nu \\
&{}^5S_2: \quad \frac{1}{2}\varepsilon^{(1)}_\mu \varepsilon^{(2)}_\nu g^\perp_{\mu\nu}\left(g^\perp_{\mu\alpha}g^\perp_{\nu\beta} + g^\perp_{\mu\beta}g^\perp_{\nu\alpha} - g^\perp_{\alpha\beta}g^\perp_{\mu\nu}\right) \\
&{}^1G_4: \quad \varepsilon^{(1)}_\mu \varepsilon^{(2)}_\nu g^\perp_{\mu\nu} X^{(4)}_{\alpha\beta\xi\eta}(q^\perp) \\
&{}^5D_4: \quad ({}^5S_2)_{\mu\nu} X^{(2)}_{\alpha\beta}(q^\perp) + symmetrisation + traceless
\end{aligned} \tag{10}$$

The product of operators for $\gamma\gamma$ and $K_sK_s$ channels leads to the following angular dependencies for partial wave amplitudes:

$$\begin{aligned}
&{}^1S_0(\gamma\gamma) \to {}^1S_0(K_sK_s): \quad 1 \\
&{}^1D_2(\gamma\gamma) \to {}^1D_2(K_sK_s): \quad \frac{1}{2}(3\cos^2\Theta - 1) \\
&{}^5S_2(\gamma\gamma) \to {}^1D_2(K_sK_s): \quad (1 - \cos^2\Theta) \\
&{}^1G_4(\gamma\gamma) \to {}^1G_4(K_sK_s): \quad \frac{1}{8}(35\cos^4\Theta - 30\cos^2\Theta + 3) \\
&{}^5D_4(\gamma\gamma) \to {}^1G_4(K_sK_s): \quad (1 - \cos^2\Theta)(7\cos^2\Theta - 1)
\end{aligned} \tag{11}$$

As well as in analysis of $e^+e^- \to e^+e^-\pi^+\pi^-\pi^0$ reaction the resonances were

parameterised as a Breit-Wigner amplitudes with the standard Blatt-Weisskopf factors.

$$A^i_{\mu\nu} = \sum_{\alpha l} \frac{g^{\alpha il}_{\gamma\gamma} g^{\alpha}_{K_sK_s}}{M^2 - s - iM\Gamma} \frac{O^{\alpha il}_{\mu\nu}}{\sqrt{F(r, k_{\gamma\gamma}, L_{\gamma\gamma}) F(r, k_{K_sK_s}, L_{K_sK_s})}} \tag{12}$$

As above the index $\alpha$ refers to the total spin of R, the indices $i, l$ to the spin and orbital angular momentum of the $\gamma\gamma$ system. There is no contribution of the triangle singularities in these reaction and we expect all couplings to be real numbers.

The operators $O^{\alpha il}_{\mu\nu}$ are calculated as the product of operators (8) and (11). For example, the ${}^5S_2(\gamma\gamma) \to^1 D_2(\mathrm{K^0_S K^0_S})$ operator is:

$$O^{220} = \frac{1}{2} \left( g^{\perp}_{\mu\alpha} g^{\perp}_{\nu\beta} + g^{\perp}_{\mu\beta} g^{\perp}_{\nu\alpha} - g^{\perp}_{\alpha\beta} g^{\perp}_{\mu\nu} \right) X_{\alpha\beta}(k^{\perp}) \tag{13}$$

# 4 Fit of the data

## 4.1 The $\mathbf{e^+e^- \to e^+e^-\pi^+\pi^-\pi^0}$ data

In the $\gamma\gamma \to \pi^+\pi^-\pi^0$ reaction the $\rho(770)$ and the $f_2(1270)$ are clearly observed in the $\pi\pi$ spectra. There is no need to introduce either $\rho_3(1690)$ or $\rho(1770)$, however a contribution from the broad state $\rho(1450)$ [8] is required to describe the data. There are no clear signals from the narrow $f$-states $f_0(980)$ and $f_0(1500)$. When these states are included in the fit their contribution appeares to be negligible, and they are omitted in the final solution. The $\pi\pi \to \pi\pi$ S-wave amplitude is included as a broad component which covers the mass region from the $\pi\pi$ threshold up to 2 GeV. It is parameterised in the framework of P-vector/K-matrix approach [10]. Only the production couplings of the two lowest K-matrix poles are varied to avoid over parameterisation of the fit.

We have performed number of fits with different combinations of resonances and background. To describe the two-pion masses and all angular distributions in the whole $W_{\gamma\gamma}$ interval we need three tensor states[1] $a_2(1320)$, $a_2(1700)$ and $a_2(2030)$, a pseudoscalar which can be identified with the $\pi(1300)$ and a $2^{-+}$ state at high $W_{\gamma\gamma}$. This hypothesis gives a good description of the $\pi^+\pi^-\pi^0$ mass spectrum, as shown in Fig. 6. A $\chi^2$ comparison gives a confidence level of 30 %. The $\pi\pi$ mass distributions, the angular distributions of pions in $\gamma\gamma$ center-of-mass system and the charged pion angular distribution in the $\pi^+\pi^-$ center-of-mass system are presented in Fig. 7 and Fig. 8 for the regions of the most prominent states, the $a_2(1320)$ and $a_2(1700)$. A $\chi^2$ comparison for these plots gives confidence levels in the range of 20 % to 40 %. If we exclude some of these states, we fail to describe the angular distributions or the branching ratios of the $a_2(1320)$ to $f_2(1270)$ and $\rho(1450)$ get unreasonably high values. To study the stability of the final solution we add one by one resonances with different quantum numbers, no other state gives a significant contribution.

[1] The names of the resonances are taken from PDG [8]

#### 4.1.1 $a_2(1320)$.

The mass and width of $a_2(1320)$, obtained by the fit, are listed in Table 1. The measured mass is 18 MeV lower than the world average [8] since in our fit the mass is the pole of the amplitude and not the central value of the mass spectrum. A fit of a Breit-Wigner with a second order polynomial background on the mass spectrum of Fig. 2a gives a values of $1312 \pm 2 \pm 10$ MeV, where the systematic error is mainly determined by cuts variation.

The $a_2(1320)$ is produced dominantly from the ${}^5S_2$ two-photon initial state. [2]

The ratio for the production from ${}^5S_2$ and ${}^1D_2$ is found to be:

$$\frac{\sigma(\gamma\gamma({}^5S_2) \to a_2(1320))}{\sigma(\gamma\gamma({}^1D_2) \to a_2(1320))} = 8.2 \pm 0.6 \tag{14}$$

According to the definitions of Ref.[7], this corresponds[3] to a ratio for the couplings $g^{\alpha ik}_{\gamma\gamma}$ of $1.30 \pm 0.25$. This value is in agreement with the theoretical expectation [11] of $0.95 \pm 0.15$, for an interaction radius of 0.6-0.8 fm.

The contribution of this resonance to the cross section is very stable in all fits, $\Gamma_{\gamma\gamma}$ is therefore well measured. The value obtained for the product of $\Gamma_{\gamma\gamma}$ with the $3\pi$ branching ratio, $Br(3\pi)$, is given in Table 1 with the statistical and systematic uncertainties.

The $a_2(1320)$ resonance dominantly decays into $\rho(770)\pi$ state in agreement with earlier analyses (see [8]). However we find that introduction of $f_2(1270)\pi$ and $\rho(1440)\pi$ decay channels improves description of the data. The contribution of these channels is found to be on the level of 5% from $\rho(770)\pi$ mode and heavily correlated with decay modes of $a_2(1700)$ state.

#### 4.1.2 $a_2(1700)$ resonance.

$a_2(1700)$ state interferes with the tail of the $a_2(1320)$. The mass, width and two-photon particle width obtained are listed in Table 1.
The resonance has a significant branching ratio into $f_2(1270)\pi$:

$$\frac{Br(a_2(1700) \to \rho(770)\pi)}{Br(a_2(1700) \to f_2(1270)\pi)} = 3.4 \pm 0.4 \tag{15}$$

This contribution is well seen on the mass slice in the resonance mass region (see Fig. 8). We also observed a possible contribution from $\rho(1450)\pi$ channel but it is much less stable due to correlation with other decay modes and the tail from the $a_2(1320)$ state.

[2] The notation ${}^{2s+1}\mathrm{L_J}$ is used here to describe the two-photon initial state

[3] This calculation involves extracting Blatt-Weisskopf barrier factors which were not introduced in [7]

The ratio for the production of the resonance from ${}^5S_2$ and from ${}^1D_2$ two-photon initial states is found to be:

$$\frac{\sigma(\gamma\gamma({}^5S_2) \to a_2(1700))}{\sigma(\gamma\gamma({}^1D_2) \to a_2(1700))} = 2.5 \pm 1.0 \tag{16}$$

The corresponding ratio of the couplings is $0.60 \pm 0.20$, well in agreement with the expectation [11] for the first radial excitation.

#### 4.1.3 $a_2(2030)$ resonance.

At higher $W_{\gamma\gamma}$ we need a contribution from another isovector tensor state defined with good accuracy from the present analysis (the mass of the state is $M = (2030 \pm 10 \pm 10)$ MeV and the width is $\Gamma = (200 \pm 22 \pm 30)$ MeV ) and it might be the same as proposed in [12]. The contribution of this resonance to the cross section is found to be stable and the product of $\Gamma_{\gamma\gamma}$ and $Br(3\pi)$, given in Table 1, is reliably calculated.

#### 4.1.4 $0^{-+}$ states and the experimental background

The likelihood value is significantly improved when a $\pi(1300)$ state is introduced in the analysis. Its contribution to the cross section is the third largest after $a_2(1320)$ and $a_2(1700)$. However the ratio between $\pi(1300)$ and $a_2(1320)$ contributions has some $P_t$ dependence which can be considered as an influence of background effects. In fact a $0^{-+}$ state, which does not interfere with $2^{++}$ states, produces a uniform angular distribution in the $\gamma\gamma \to \pi^+\pi^-\pi^0$ reaction similar to that from the background contribution. Considering that the signal to noise ratio is rather low in the mass region below 1.2 GeV, as shown on Fig. 1a, we can only estimate an upper limit for the $\gamma\gamma$ width of this state. This is listed in Table 1 together with the fitted values of mass and width.

#### 4.1.5 $\pi_2$ signal.

A $2^{-+}$ signal is found in the mass region 1850-1900 MeV. It can be partly related to $\pi_2(1670)$ [8]. However, fixing the $2^{-+}$ signal to the parameters of $\pi_2(1670)$ makes the likelihood worse and if the mass is left free it always moves to the 1850-1900 MeV where the signal becomes stronger. Therefore from the present analysis we can only give an upper limit for the $\gamma\gamma$ width of $\pi_2(1670)$ and to point out a possible presence of a $2^{-+}$ signal in 1850-1900 MeV mass region. These values are given in Table 1.

#### 4.1.6 Contribution of different states

The individual contributions to the cross section $\gamma\gamma \to \pi^+\pi^-\pi^0$, proportional to $\mid A^i_{\mu\nu} \mid^2$, are shown in Fig. 9. The sum of the amplitudes squared differs from

the total cross section, due to interference between overlapping $2^{++}$ states. The resonance masses obtained from the fit are corrected for an instrumental effects found from MC simulation. Masses are decreased by 1 MeV for the $a_2(1320)$ and by 6 MeV for the $a_2(2030)$. The experimental resolution in masses measurement is (5-6) MeV and does not influence on the width of a resonance.

## 4.2 The $e^+e^- \to e^+e^-K^0_S K^0_S$ data

The mass distribution from $\gamma\gamma \to K_sK_s$ reaction is shown in Fig. 5 and the angular distribution for the total mass region in Fig. 11a. It is immediately seen that the angular distribution follows very close to the $(1-\cos^2\Theta)^2$ shape. However due to our acceptance which falls rapidly at large $\cos\Theta$ it is very difficult to distinguish between a tensor and a scalar state. This might be the main reason why the partial wave analysis gives quite often solutions with some admixture of the (nonresonant) S-wave.

There is no doubt about the structure of the $K_sK_s$ mass distribution below 1600 MeV: the states of the first tensor nonet are clearly seen. In the analysis we use the model [11] already confirmed during consideration of the $\gamma\gamma \to \pi^+\pi^-\pi^0$ reaction. The model provides the ratio between $^5S_2$ and $^1D_2$ waves as well as $\gamma\gamma$ couplings which are calculated from a triangle quark diagram. In this calculation, the $\gamma\gamma$ width of $a_2(1320)$ (see Fig. 12a) reproduces the experimental value at $R^2 = (8 \pm 1.5)$ GeV$^{-2}$ ($R = 0.56 \pm 0.1$ fm). The dependence of the $\gamma\gamma$ widths of the lowest isoscalar tensor mesons on mixing angle is shown in Fig. 12b.

We calculate $K^0_S K^0_S$ coupling for the first tensor nonet using the $K\bar{K}$ width of $f_2'(1525)$. Partial $K^0_S K^0_S$ widths of the $a_2(1320)$ and $f_2(1270)$ resonances are determined from $SU(3)$ relations, the first nonet masses are taken from PDG. The $K_sK_s$ mass spectrum under these assumptions is shown in Fig. 13a. It is clearly seen that it reproduces reasonably well the interference in the mass region around 1.3 GeV and the $f_2'(1525)$ peak, but certainly, improvements are necessary.

For the description of isoscalar S-wave resonances we use the P-vector approach with K-matrix parameterisation taken from [13]. There are no free parameters in this amplitude apart from a smooth nonresonance production. We find that introduction of the nonresonant $\gamma\gamma \to \pi^+\pi^-$ transition improves likelihood. However such contribution makes only a marginal change in $K_sK_s$ mass spectrum description: as well as for $\pi\pi \to K\bar{K}$ data [14] S-wave rapidly decreases at higher energies and in the region around 1700 MeV produce almost negligible contribution.

The $a_0(980)$ state is parameterised as Flatté form with coupling to $\pi\eta$ and $K\bar{K}$ channels. The $\gamma\gamma$ widths of the states are calculated as described in [11].

A contribution from $4^{++}$ states is seen from angular distribution at high energies (Fig. 11). The fit does not determine the mass and width of a resonance. To solve this problem we introduce in addition a nonresonant $4^{++}$ wave contribution. It turned out to be very small (less then 1% from total cross section) but the $4^{++}$ resonance contribution now gives a narrow state with mass $(2150 \pm 30)$ MeV and

width $(50 \pm 20)$ MeV. This can be an indication of a dominantly $s\bar{s}$ $4^{++}$ state. However on the basis of the present statistics, we can not exclude a statistical fluctuation.

A nonresonant $2^{++}$ contribution is also found to be useful to describe the data. It does not change the main features of the picture but provides an improvement in likelihood. The description of the data is shown in Fig. 13b: this is starting point for the investigation of the (1700-1800) MeV mass region.

First we introduce a scalar state $f_0(1710)$ with the mass and the width as free parameters. The fit fails to reproduce a structure in 1700-1800 MeV mass region. The description of the data is shown in Fig. 13c. The mass is estimated as (1805±30) MeV and width $(260 \pm 30)$ MeV. With such mass and width, the $f_0$ state describes only the slope in mass distribution above 1800 MeV.

At the next step we have introduced the $f_0(1710)$ state with fixed mass and width from PDG: $M = 1709$ MeV and $\Gamma = 120$ MeV. Such fit fails immediately. Indeed, the data have a minimum in the region 1710 MeV while the resonance produces a maximum in this region. The fit has slightly better likelihood if mass is fixed at the latest BES value [15] $M = 1740$ MeV. However the result is still not a satisfactory one and is shown in Fig. 13d.

The main problem in fits with $f_0$ states is that there is no way to reproduce a dip in the 1700 MeV region and slope above 1800 MeV. We have tried to introduce a constant width, a width defined by the $K\bar{K}$ channel and a width defined by $K^*\bar{K}^*$ channel. The situation is even worse in the later two cases. A $f_0$ state can only interfere with ${}^1D_2$ component of a $2^{++}$ state and this partial wave is very small in the data. As the result $f_0$ and $f_2$ contributions do not interfere even on the amplitude level and of course are added incoherently on the level of the cross section. This leads to filling the dip in the region 1700 MeV.

With a tensor state in the region 1750 MeV we immediately find good description of the mass spectrum (Fig. 10). The mass of the state is found to be $(1755 \pm 10)$ MeV and the width $(67 \pm 12)$ MeV. The fit describes well the dip between $f_2'(1525)$ and $f_2(1750)$ states. Contrary to the fit with the scalar meson $f_0(1710)$, the $f_2(1750)$ resonance interferes naturally with tails of other tensor states, producing a dip and good description of this mass region.

Let us remark that during the partial wave analysis described above , fits are also performed when the first tensor nonet parameters are free, without SU(3) restrictions, however all parameters do not move for more then 20% from SU(3) values.

# 5 $SU(3)$ properties of the mesons

Let us consider production and decay properties of the isospin 0 and isospin 1 states on the basis of a quark model.

The meson states consisting of light quarks $n = u, d$ and strange quarks $s$ form meson nonet: three isospin 1 -pions, four isospin $\frac{1}{2}$ - kaons and two isoscalar states

$\eta$ and $\eta'$ mesons. The isoscalar states can be a mixture of $n\bar{n}$ and $s\bar{s}$ components:

$$\begin{aligned} \eta &= n\bar{n}\cos\Theta - s\bar{s}\sin\Theta \\ \eta' &= n\bar{n}\sin\Theta + s\bar{s}\cos\Theta, \end{aligned} \tag{17}$$

where $\Theta$ is the nonet mixing angle for $\eta - \eta'$ mesons .

Similar consideration is valid for a tensor nonet.

An isospin 1 state has a $(u\bar{u} - d\bar{d})/\sqrt{2}$ quark structure and the component of isospin 0 without strange quarks has structure $(u\bar{u} + d\bar{d})/\sqrt{2}$. The decay of such states into two kaons is defined by the production of an $s\bar{s}$ pair ( s-quark exchange) and has the following structure:

$$\begin{aligned} \frac{u\bar{u} + d\bar{d}}{\sqrt{2}} &\rightarrow K^+K^- + K^0\bar{K}^0 \\ \frac{u\bar{u} - d\bar{d}}{\sqrt{2}} &\rightarrow K^+K^- - K^0\bar{K}^0 \end{aligned} \tag{18}$$

If an isoscalar dominantly nonstrange state and an isospin 1 state have similar masses one should observe a strong destructive interference in the neutral kaon channel. Of course it would be extremely interesting to perform a combined analysis of the neutral and charged kaon final states: in the latter case the interference would be constructive and the couplings can be fixed from such analysis with an extremely good accuracy.

The $s\bar{s}$ component of isospin 0 state decays into kaons by $u$- and $d$-quark exchange. The calculation of different decay modes shows that the s-quark exchange is suppressed compare to the nonstrange quark exchange by a factor $\lambda = (0.75 - 0.85)$. Thus, we expect a stronger kaon production from dominantly $s\bar{s}$ states. A real isospin 0 state can be a mixture of nonstrange and strange components and ratios for decay of such state into different two body channels (as well as ratios for isovector states) are given in the Table 2.

If SU(3) is conserved, all members of a nonet have the same masses and coupling constant. Violation of SU(3) leads to a larger mass of strange quark and some changes of quark interaction properties. It is reflected by mass splitting inside nonets and in some cases to nontrivial final state interaction effects, when position of meson thresholds plays a significant role. However nonets properties such as systematic and similarity of wave functions are not strongly violated. It means that decays of the resonances into two body channels can be described with a good accuracy by the same nonet coupling after extracting phase space and Blatt-Weisskopf factors.

If quark wave functions of the states are similar (as expected for the nonet members) the $\gamma\gamma$ widths of these states are different only by the quark charge and phase space effects. So we expect that an isoscalar $n\bar{n}$ state has the $\gamma\gamma$ width which is 25/9 larger than an isospin 1 state and 25/2 times larger than a $s\bar{s}$ state. Indeed the $f_2(1270)$ resonance has a $\gamma\gamma$ width $(2.6 \pm 0.24)$ KeV [8] while $a_2(1320)$ has $(0.90 \pm$

0.06) KeV, in agreement with the assumption that $f_2(1270)$ is a dominantly $n\bar{n}$ isoscalar state. The $\gamma\gamma$ width of $f_2'(1525)$ is not well known. The Argus collaboration found that exact number depends strongly on the assumptions about how this state interferes with the background [16].

## 5.1 The first nonet of tensor mesons

The first nonet of tensor mesons (the states with ground radial wave function) is formed by: $a_2(1320)$, $K_2(1430)$,$f_2(1270)$ and $f_2'(1525)$.

All these states are well known and many of their properties were investigated in details, e.g. in $\pi^- p \to \pi\pi n$ reactions [18, 19]. The dominant decay mode of $f_2(1270)$ meson is into $\pi\pi$ channel. The $K\bar{K}$ signal from this state is rather weak due to small D-wave phase space factor. As the result the $K\bar{K}$ coupling is defined with much larger error.

The main decay mode of $a_2(1320)$ state is $\rho\pi$ channel contributing $70.1 \pm 2.7\%$ [8] of the total width of this state. Probably the best determination of the mass and width of this state was done by the VES collaboration [20]. The second strongest decay mode of $a_2(1320)$ is into the $\pi\eta$ channel ($14.5 \pm 1.2\%$ ) [8].

The $f_2'(1525)$ resonance mainly decays into the $K\bar{K}$ channel. The decay probability is quite suppressed by the D-wave phase space and this explains why this state is expected to bea narrow one: its width is $(76 \pm 10)$ MeV [8]. However we should remark that in many analyses the width of this state was found to be larger: about 100 MeV (see references given in PDG [8]).

The SU(3) properties of decays of the lowest tensor mesons into two pseudoscalar mesons and $\gamma\gamma$ channel were studied in [11, 17]. It was shown that using the same coupling , the mixing angle and the radius of the states one can described the two body partial widths of tensor resonances with a good accuracy: 15%-20%.

Thus, in our analysis with SU(3) relation imposed we fit common nonet coupling and mixing angle to describe decays of the tensor states into two pseudoscalars. Following calculations [17], for the description of $K\bar{K}$ channel we introduce as parameters, the SU(3) violation factors. We find that this factor is largest for the $a_2(1320)$ state reaching 15% (see Table 4) close to the PDG value. The mixing angle between nonstrange and $s\bar{s}$ components of the first tensor nonet is found to be very close to zero: $(-1 \pm 3)$ degrees. The fit is very sensitive to this value.

In paper of Anisovitch et al [11] two solutions produced similar results for the $\gamma\gamma$ widths for first three tensor states: one with the mixing angle between around 0 degrees and another solution with the mixing angle of 25 degrees (see Fig. 12b). It is seen that the $\gamma\gamma$ coupling of $f_2'(1525)$ crosses zero at 16 degrees and amplitudes calculated at 0 and 25 degrees have different sign. The sign plays no role in the calculation of the $\gamma\gamma$ width, but due to interference between all tensor mesons in the present data the fit is quite sensitive to it. As the result the negative sign of the $\gamma\gamma$ coupling for production of $f_2'(1525)$ state is strongly forbidden by the data: the description of the data with mixing angle 25 degrees is shown in Fig. 14a.

In paper [17] the SU(3) characteristics for the first tensor nonet were defined from the fit of large number of two meson decay modes. The mixing angle was found to be $(7 \pm 2)$ degrees . This value is not very far from our result but there is an important difference. Due to fast variation, the $\gamma\gamma$ coupling of $f_2'(1525)$ becomes very small already at 7 degrees (see Fig. 12b). The $K\bar{K}$ coupling is also strongly decreased at positive mixing angle. As the result it is very difficult to reproduce well a peak from the $f_2(1525)$ state. The description of data with the fixed 7 degrees mixing angle is shown in Fig. 14b. Let us remark that the suppression factor from $s\bar{s}$ phase space (which is about 2) plays significant role here. If it was not taken into account then our results are shifted by 3-4 degrees in positive region and the errors overlap with errors given in [17].

## 5.2 The second tensor nonet

The best candidate for the first radial excitation of tensor states is $f_2(1565)$ which was observed by many collaborations [21], [22],[23],[24], [25]. One of the most detailed investigation had been done by Crystal Barrel collaboration. The resonance was observed in $p\bar{p} \to 3\pi$ and $p\bar{p} \to \omega\omega\pi$ reactions and the mass was defined to be $(1570 \pm 25)$ MeV. The resonance couples strongly to $\omega\omega$ channel and its pole is attracted to the $\omega\omega$ threshold by Flatté effect.

The decay of $f_2(1565)$ into $\pi\pi$ channel was observed in several experiments but the $\pi\pi$ partial width was not defined. The limit for the width was defined by the data from $\pi\pi$ production experiments: CERN-Münich [18], GAMS [19]. Here the $\pi\pi n$ final state is produced from interaction of high energy $\pi^-$ with proton and the data selected at very small transfer energies provide information about $\pi\pi \to \pi\pi$ amplitude close to the unitarity limit. The isoscalar tensor amplitude can be clearly extracted and it had no significant structure in the region higher $f_2(1270)$: the limit 30 MeV comes from uncertainties in the measured cross section.

In our analysis we used the parameterisation of $f_2(1565)$ found by Crystal Barrel collaboration in $p\bar{p}$ annihilation at rest [22],[23].

The $a_2(1700)$ state was first observed by L3 collaboration [27] and then by Crystal Barrel collaboration. From analysis of the L3 data the mass was found to be $(1752 \pm 21 \pm 4)$ MeV [27]. In the Crystal Barrel analysis of the $\bar{p}p$ annihilation at rest into $\pi\pi\eta$, made under assumption about 100% annihilation from S-wave the mass and width of this state was found to be $(1660 \pm 40)$ MeV and $(280 \pm 70)$ MeV respectively. However after including P-wave annihilation the fitted mass moved to a higher value [28]. The same result was found in $\bar{p}p$ annihilation in flight. In this reaction the mass was determined as $(1698 \pm 44)$ MeV [29]. With significant increase of the statistics, L3 collaboration has confirmed the existence of $a_2(1700)$ state and the mass moved to $(1722 \pm 9 \pm 8)$ MeV and the width was found to be $(340 \pm 20 \pm 20)$ MeV [4], in a good agreement with latest Crystal Barrel results.

We can assume that $f_2(1565)$ and $a_2(1700)$ together with isoscalar $f_2(1750)$ are members of the same nonet: second nonet of tensor mesons.

## 5.3 The nonet approach to the analysis of the $\gamma\gamma \to \mathrm{K^0_S K^0_S}$ data.

Thus, in our analysis with SU(3) relation imposed we fit the nonet coupling and mixing angle to describe decays of the tensor states into two pseudoscalars.

We fix parameters for $f_2(1560)$ from the Crystal Barrel results and for $a_2(1700)$ from the our analysis of the $\pi^+\pi^-\pi^0$ channel. At given mixing angle the nonet coupling was calculated to reproduce the $\pi\pi$ width of 25 MeV for the $f_2(1560)$ state. Then free parameters for this nonet are the mixing angle and the mass and width of $f_2(1750)$. We did not observe any visible dependence on the radii of the states. The main reason is that $K\bar{K}$ threshold is rather remote from the resonance position and the Blatt-Weisskopf factors almost canceled when $K\bar{K}$ width of the $f_2(1750)$ state is calculated out of the $\pi\pi$ width of $f_2(1560)$ state. Therefore we fixed the radius of second nonet states from results of calculations [11]. We also performed a set of fits when $\pi\pi$ width of $f_2(1560)$ resonance was fixed at 20 MeV. We find that in this case the likelihood minimum value corresponds to mixing angle shifted by 3 degrees in the negative direction.

We find very good description of the data with $SU(3)$ relations imposed. The likelihood has the same value and quality of the fit is the same as the fit without $SU(3)$ relations described in the previous section. The masses, widths, radii, $K\bar{K}$ couplings, mixing angles and partial widths of the states are given in Tables 3,4 and the description of the data is shown in Fig. 10-11. The $\gamma\gamma$ width of the $f_2(1270)$ state is found to be in a good agreement with PDG value [8], and the $\gamma\gamma$ width of $f_2(1750)$ state defined with a good accuracy (see Table 4).

The $f_2(1560)$ and $a_2(1700)$ states practically do not contribute to the cross section of the process $\gamma\gamma \to \mathrm{K^0_S K^0_S}$ . The $f_2(1750)$ state has mass $(1755 \pm 10)$ MeV and total width $(67 \pm 12)$ MeV. Its $K\bar{K}$ width is $(23 \pm 7)$ MeV and the rest of the width is likely to be defined by the $K^*\bar{K}$ channel. This resonance destructively interferes with tail from $f_2'(1525)$ state creating the dip in the mass region 1700 MeV. When the sign of the real part of the $f_2(1750)$ amplitudes changes this interference becomes positive producing a clear peak in the data.

The mixing angle of the second nonet is found to be $-10^{+5}_{-10}$ degrees.

A description of the data in the framework of the nonet approach has a significant problem if peak at 1750 MeV is assumed to be due to a scalar state. If this state is a nonet partner of one of the known states, e.g.$f_0(1370)$ or $f_0(1500)$, then the calculated signal is too weak to fit the data. If the $K\bar{K}$ coupling of this scalar state is fitted free, we found that it must be about 4 times bigger then the total width of the resonance. This is due to $2J + 1$ suppression factor and absence a positive interference with tail of $f_2'(1525)$ which boosts the peak in the case of tensor state. These problems are additional to that connected with description of the dip in the 1700 MeV region.

# 6 Is position of the tensor states an indication for presence of a glueball?

There is no doubt that we have defined two tensor nonets with a good accuracy. However there is an important question: why masses of the tensor isoscalar states are systematically lower then masses of isovector states. Such a phenomenon is not present in the $J^{PC} = 1^{--}$ sector where masses of $\rho$-states are very close to masses of $\omega$-states. In the tensor sector, the mass of $f_2(1270)$ is 30-35 MeV lower then the $a_2(1320)$ mass and the mass of $f_2(1560)$ is more then 100 MeV lower then mass of $a_2(1700)$. A Flatté form of $f_2(1560)$ allows some flexibility to increase the K-matrix mass (bare mass) of the state. However the shift can not be larger then 20-30 MeV. The mass of $f_2(1750)$ somehow supports the mass position of the $f_2(1560)$ state: it is situated about 200 MeV higher. The mass shift between $f_2(1560)$ and $a_2(1700)$ can not be explained due to mixing of nonstrange and strange components in isoscalar sector: in such mixing the average mass squared does not change and we should find $f_2(1750)$ at a much higher mass. Instead we observe a shift of both isoscalar states down in mass.

Such phenomenon can be an indication for the presence of a tensor glueball in the mass region 1800-2000 MeV. The interference of quark-antiquark mesons with such a state (which has decay properties similar to a $q\bar{q}$ singlet state) could shift down masses of all isoscalar members of the first two nonets. And such shift would be stronger for the second tensor nonet situated closer to the glueball state. An observation of a tensor state in mass region with glueball properties was reported in [15] from analysis of $J/\Psi$ decay data and a confirmation of its existence is a very important task.

# 7 Summary

The high statistics sample of $e^+e^- \to e^+e^-\pi^+\pi^-\pi^0$ data collected by L3 at LEP allows an accurate amplitude analysis of the three pion final state. In addition to the dominant $a_2(1320)$ we have to consider two more isovector tensor states $a_2(1700)$ and $a_2(2030)$. They can be interpreted as the $a_2(1320)$ radial excitations. The presence of a $0^{-+}$ and a $2^{-+}$ waves is also necessary to describe the data, but the instability of their parameters do not allow a clear resonance interpretation.

Partial wave analysis of $\gamma\gamma \to \mathrm{K^0_S K^0_S}$ proves that the peak at 1750 MeV is due to a tensor state. Although a scalar state is not forbidden by the experimental angular distributions it fails to describe simultaneously the dip in the region of 1700 MeV and the slope higher 1750 MeV. The $f_2(1750)$ is fitted with well determined mass and width. If nonet relations are applied this state is revealed as a solid member of the second tensor nonet together with $f_2(1560)$ and $a_2(1700)$ states. The data defines very well mixing angles for two tensor nonets which are $(-1 \pm 3)$ degrees for the first tensor nonet and $(-10^{+5}_{-10})$ for the second tensor nonet.

# 8 Acknowledgments

We are very grateful to V.V. Anisovich and E. Klempt for extremely useful discussions and comments. A.V. Sarantsev acknowledges support from Science support foundation (grant for talented young researches).

# References

[1] L3 Coll., B. Adeva et al., Nucl. Instr. and Meth. **A 289** (1990) 35;
M. Acciarri et al., Nucl. Instr. and Meth. **A 351** (1994) 300;
M. Chemarin et al., Nucl. Instr. and Meth. **A 349** (1994) 345;
A. Adam et al., Nucl. Instr. and Meth. **A 383** (1996) 342.

[2] P. Béné et al., NIM **A 306** (1991) 150

[3] D. Haas et al., NIM **A 420** (1999) 101.

[4] V.Schegelsky et al., L3 Note 2798,May 8,2003; V.Schegelsky et al., L3 Note 2799,May 8,2003. To be published in Phys Lett.

[5] V.V. Anisovich et al., Phys.Atom.Nucl 57 (1994) 1595.

[6] F. Von Hippel and C. Quigg, Phys. Rev. D **5** (1972) 624.

[7] A.V. Anisovich et al., hep-ph/0105330.

[8] K. Hagiwara et al. (Particle Data Group), Phys. Rev. D **66** (2002) 1.

[9] A. V. Anisovich, V. V. Anisovich, V. N. Markov, M. A. Matveev and A. V. Sarantsev, J. Phys. G **28** (2002) 15, hep-ph/0105330.

[10] V.V. Anisovich, Yu.D. Prokoshkin and A.V. Sarantsev. Phys.Lett. B 389 (1996) 388, hep-ph/9610414.

[11] A.V. Anisovich, V.V. Anisovich, M.A. Matveev, V.A. Nikonov. Apr 2002. 37pp. "Two photon partial widths of tensor mesons", hep-ph/0204330

[12] A. Anisovich et al. Phys.Lett. **B**517 (2001) 261.

[13] V. V. Anisovich and A. V. Sarantsev, Eur. Phys. J. A **16** (2003) 229, hep-ph/0204328.

[14] S. J. Lindenbaum and R. S. Longacre, Phys. Lett. **B274**, 492 (1992);

[15] J.Z. Bai et al., (BES collaboration), Phys. Lett. **B**472 (2000) 207.

[16] H. Albrecht et al. (Argus collaboration), Z.Phys. **C**48 (1990) 183.

[17] E. Klempt, K. Peters (Mainz U., Inst. Phys.).

[18] B. Hyams et al., Nucl. Phys. **B64** (1973) 134.

[19] F. Binon et al., Nuovo Cim. **A80** (1984) 363.

[20] VES Collaboration, D. Amelin et al., Z. Phys. **C70** (1996) 71.

[21] P. Weidenauer *et al.* [ASTERIX Collaboration.], Z. Phys. C **59** (1993) 387.

[22] Crystal Barrel, V.V. Anisovich et al., **B323** (1994) 233.

[23] C.A. Baker et al., Phys.Lett. **B467** (1999) 147.

[24] Obelix collaboration, Bertin et al., Phys. Rev., D57 (1998) 55; Phys.Lett. **B408** (1997) 476.

[25] VES Collaboration, D. Amelin et al., Nucl. Phys. **B668** (2000) 83.

[26] The CRYSTAL BARREL Collaboration (C. Amsler et al.), Phys. Lett. B322 431, (1994).

[27] M. Acciarri et al., (L3 collaboration) Phys.Lett. **B**413 (1997) 147.

[28] E. Klempt and A. Sarantsev, private communication.

[29] C. Amsler et al., (Crystal barrel) E.Phys.J., **C**23 (2002) 29.

Table 1: Masse, width and the product of $\Gamma_{\gamma\gamma}$ times $Br(3\pi)$ for the observed resonances. The name of the resonances is taken from Ref. [8]

| Resonance | M (MeV) | $\Gamma$(MeV) | $\Gamma_{\gamma\gamma}Br(3\pi)$(keV) |
|---|---|---|---|
| $a_2(1320)$ | $1300 \pm 2 \pm 2$ | $117 \pm 6 \pm 10$ | $0.65 \pm 0.02 \pm 0.02$ |
| $a_2(1700)$ | $1722 \pm 9 \pm 8$ | $336 \pm 20 \pm 20$ | $0.37^{+0.12}_{-0.08} \pm 0.10$ |
| $a_2(2030)$ | $2050 \pm 10 \pm 10$ | $190 \pm 22 \pm 30$ | $0.11 \pm 0.04 \pm 0.05$ |
| $\pi(1300)$ | $1345 \pm 8 \pm 10$ | $260 \pm 20 \pm 30$ | $\leq 0.8(95\%CL)$ |
| $2^{-+}$ | $1860 \pm 12 \pm 10$ | $352 \pm 30 \pm 40$ | $0.15 \pm 0.03 \pm 0.05$ |
| $\pi_2(1670)^*$ | 1670 | 260 | $\leq 0.1(95\%CL)$ |

$^*$ - the $2^{-+}$ signal is fixed as $\pi_2(1670)$ with values taken from Ref. [8].

Table 2: Coupling constants given by quark combinatorics for a $q\bar{q}$-meson decaying into two pseudoscalar mesons in the leading terms of the $1/N$ expansion. $\Phi$ is the mixing angle for $n\bar{n} = (u\bar{u} + d\bar{d})/\sqrt{2}$ and $s\bar{s}$ states, and $\Theta$ is the mixing angle for $\eta - \eta'$ mesons: $\eta = n\bar{n}\cos\Theta - s\bar{s}\sin\Theta$ and $\eta' = n\bar{n}\sin\Theta + s\bar{s}\cos\Theta$.

| Channel | The $q\bar{q}$-meson decay couplings for isospin=0 tensor states | The $q\bar{q}$-meson decay couplings for isospin=1 tensor states | Identity factor in phase space |
|---|---|---|---|
| $\pi^0\pi^0$ | $g\ \cos\Phi/\sqrt{2}$ | | 1/2 |
| $\pi^+\pi^-$ | $g\ \cos\Phi/\sqrt{2}$ | | 1 |
| $\eta\pi^0$ | | $g\ \frac{1}{\sqrt{2}}\cos\Theta$ | 1 |
| $K^+K^-$ | $g(\sqrt{2}\sin\Phi + \sqrt{\lambda}\cos\Phi)/\sqrt{8}$ | $g\sqrt{\lambda}/\sqrt{8}$ | 1 |
| $K^0K^0$ | $g(\sqrt{2}\sin\Phi + \sqrt{\lambda}\cos\Phi)/\sqrt{8}$ | $g\sqrt{\lambda}/\sqrt{8}$ | 1 |
| $\eta\eta$ | $g\big(\cos^2\Theta\ \cos\Phi/\sqrt{2} + \sqrt{\lambda}\ \sin\Phi\ \sin^2\Theta\big)$ | | 1/2 |
| $\eta\eta'$ | $g\sin\Theta\ \cos\Theta\big(\cos\Phi/\sqrt{2} - \sqrt{\lambda}\ \sin\Phi\big)$ | | 1 |
| $\eta'\eta'$ | $g\big(\sin^2\Theta\ \cos\Phi/\sqrt{2} + \sqrt{\lambda}\ \sin\Phi\ \cos^2\Theta\big)$ | | 1/2 |

Table 3: Coupling constants, mixing angles and decay widths for the first tensor nonet calculated from the $SU(3)$ fit. Values with star were fixed from another data.

| | First nonet | | |
|---|---|---|---|
| | $a_2(1320)$ | $f_2(1270)$ | $f_2'(1525)$ |
| Mass (MeV) | $1304 \pm 10$ | $1277 \pm 6$ | $1523 \pm 5$ |
| Width (MeV) | $120 \pm 15$ | $195 \pm 15$ | $104 \pm 10$ |
| $KK$ width (MeV) | $7.0^{+2.0}_{-1.5}$ | $7.5 \pm 2$ | $68^*$ |
| Nonet coupling (GeV) | $0.95 \pm 0.08$ | | |
| $SU(3)$ violation factor | $0.85 \pm 0.1$ | $0.95 \pm 0.1$ | $1.1 \pm 0.1$ |
| Mixing angle (degrees) | $-1 \pm 3$ | | |
| $\gamma\gamma$ width (KeV) | $0.91^*$ | $2.55 \pm 0.15$ | $0.13 \pm 0.03$ |
| $\pi\pi$ width (MeV) | | $152 \pm 8$ | $0.2^{+1.0}_{-0.2}$ |
| $\pi\eta$ width (MeV) | $18.5 \pm 3$ | | |
| $\eta\eta$ width (MeV) | | $1.8 \pm 0.4$ | $5.0 \pm 0.8$ |

Table 4: Coupling constants, mixing angles and decay widths for the second tensor nonet calculated from the $SU(3)$ fit. Values with star were fixed from another data.

| | Second nonet | | |
|---|---|---|---|
| | $a_2(1700)$ | $f_2(1560)$ | $f_2(1750)$ |
| Mass (MeV) | $1722^*$ | $1570^*$ | $1755 \pm 10$ |
| Width (MeV) | $336^*$ | $160^*$ | $67 \pm 12$ |
| $K\bar{K}$ width (MeV) | $5 \pm 3$ | $2 \pm 1$ | $17 \pm 5$ |
| Nonet coupling (GeV) | $0.35 \pm 0.05$ | | |
| $SU(3)$ violation factor | $1.^*$ | | |
| Mixing angle (degrees) | $-10^{+5}_{-10}$ | | |
| $\gamma\gamma$ width (KeV) | $0.30 \pm 0.05$ | $0.70 \pm 0.14$ | $0.13 \pm 0.04$ |
| $\pi\pi$ width (MeV) | | $25^*$ | $1.3 \pm 1.0$ |
| $\pi\eta$ width (MeV) | $9.5 \pm 2$ | | |
| $\eta\eta$ width (MeV) | | $1.2 \pm 0.3$ | $2.0 \pm 0.5$ |

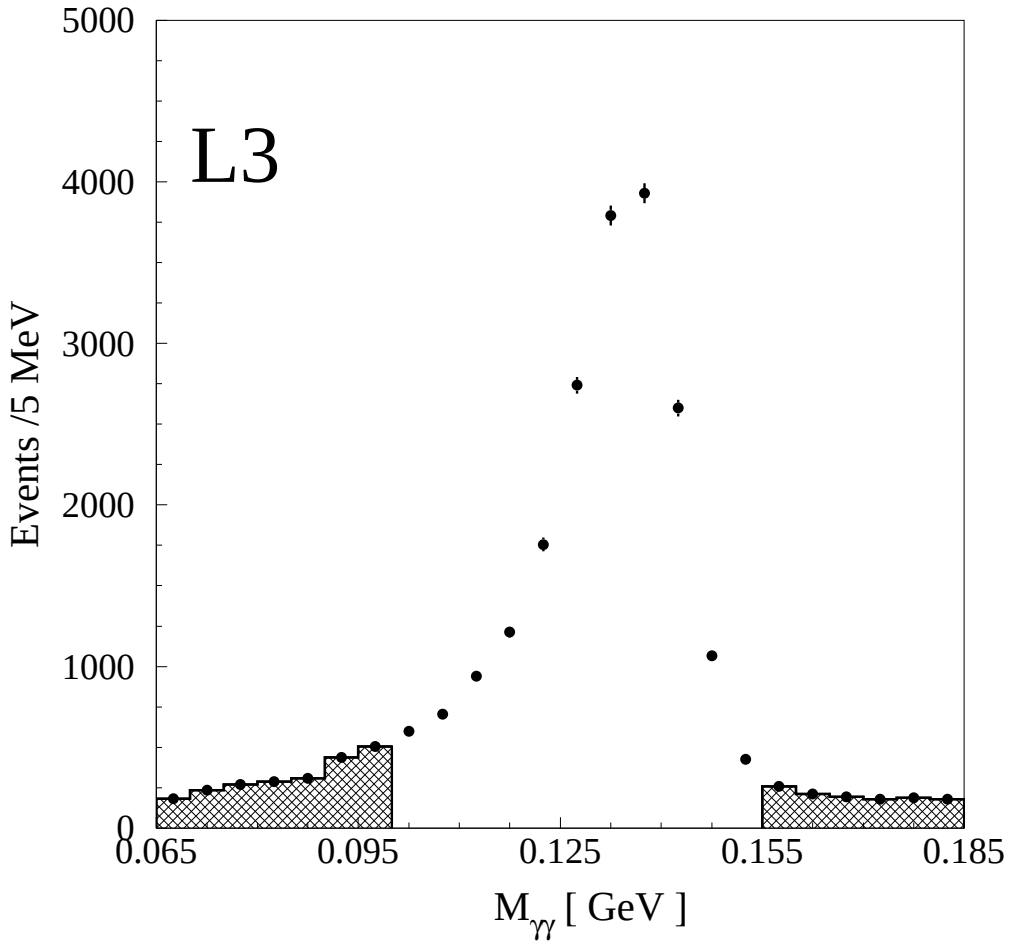


Figure 1: Effective mass of two candidate photons. The side bands of the $\pi^0$, used to evaluate the background, are indicated as shaded areas.

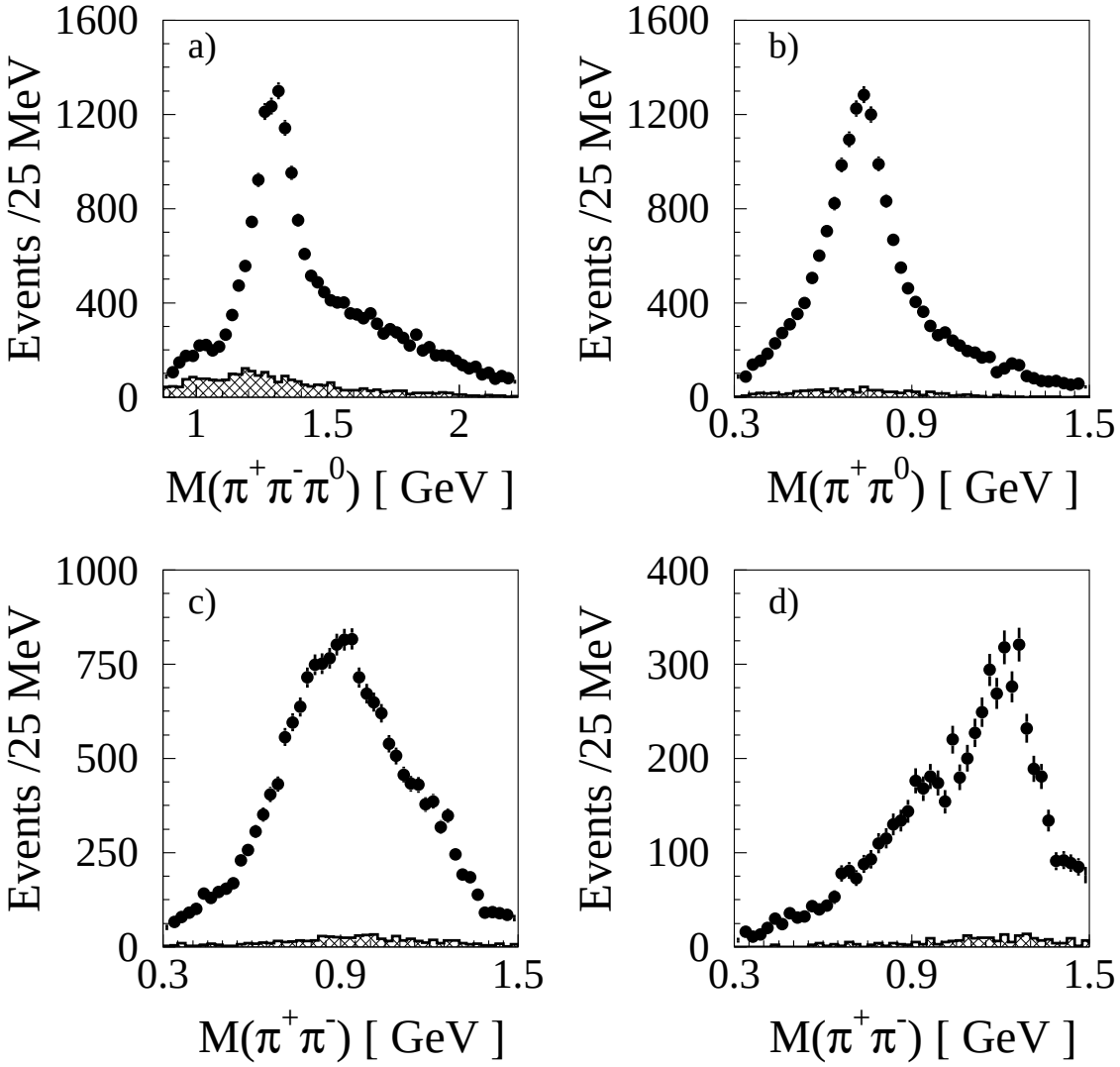


Figure 2: Mass spectra with cuts $P_t < 0.1$ GeV and $P_t^c > 0.05$ GeV, a) $M(\pi^+\pi^-\pi^0)$; b) $M(\pi^\pm\pi^0)$; c) $M(\pi^+\pi^-)$; d) $M(\pi^+\pi^-)$ with 3 pion mass higher than 1.5 GeV; The background, estimated from the side bands of the $\pi^0$, is shown as a shaded area.

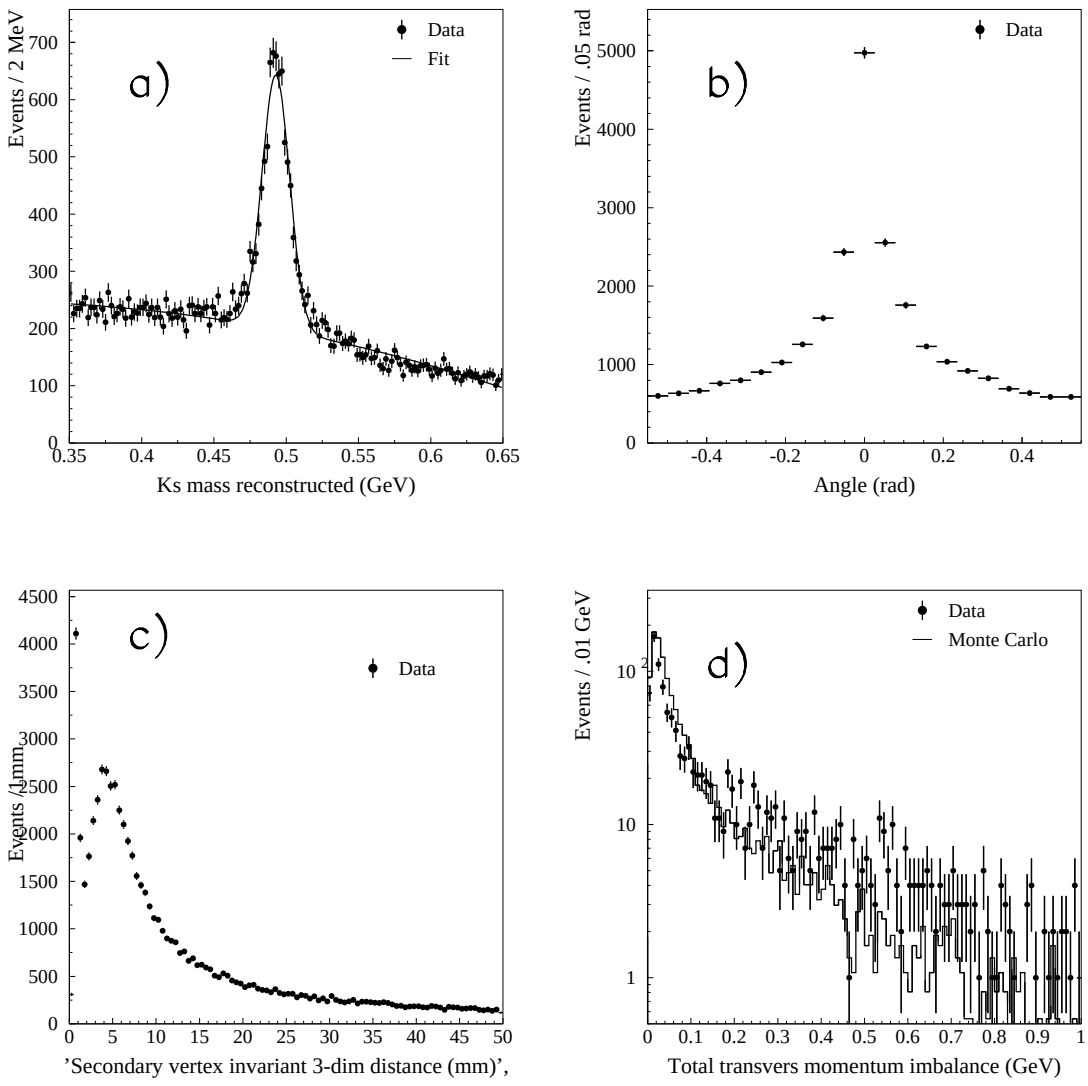


Figure 3: a) The $\pi^+\pi^-$ mass spectrum for reconstructed secondary vertices; b) The angle between the flight direction and the total transverse momentum for the $K^0_S$ candidates; c) invariant 3-dimensional distance between the primary and the secondary vertex; d) The total transverse momentum imbalance .

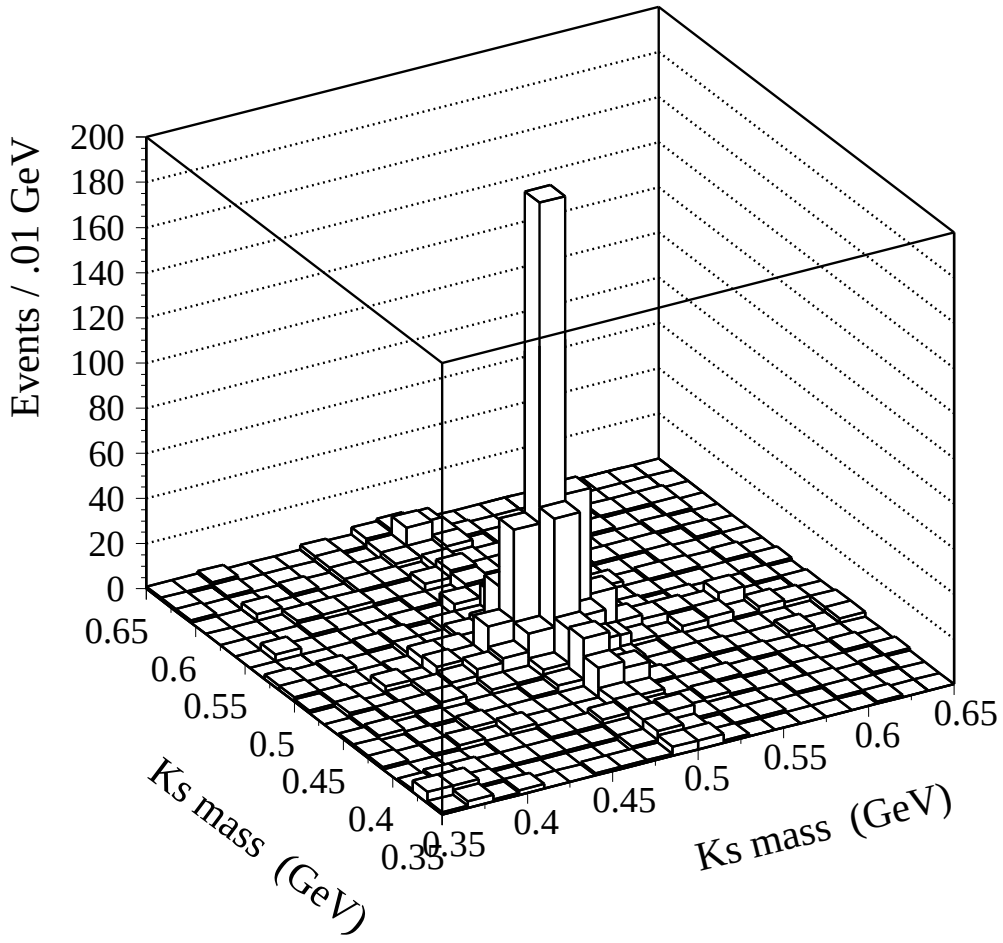


Figure 4: The distribution of the mass of one $K_s$ candidate versus the mass of the other candidate.

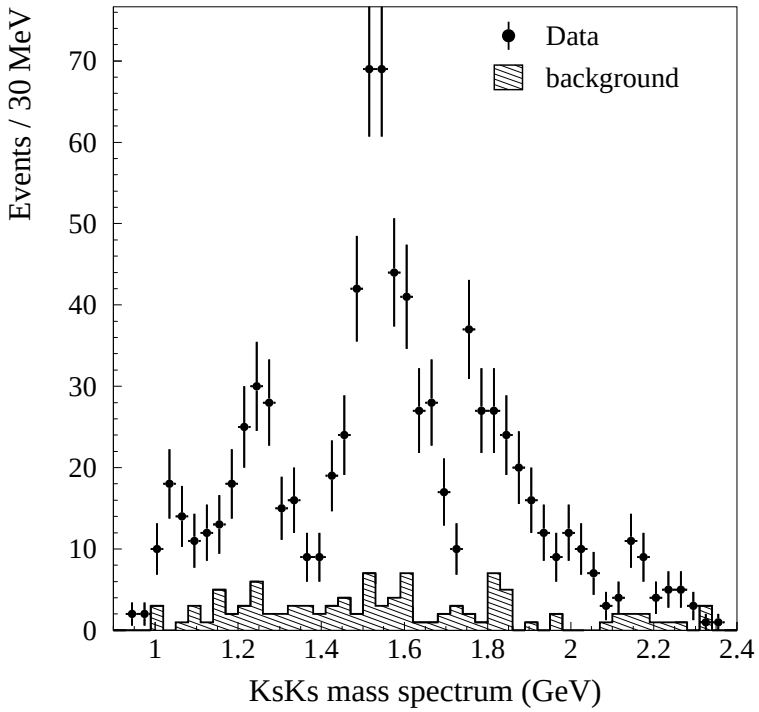


Figure 5: The $K_sK_s$ mass spectrum of selected events with the mass spectrum of the background.

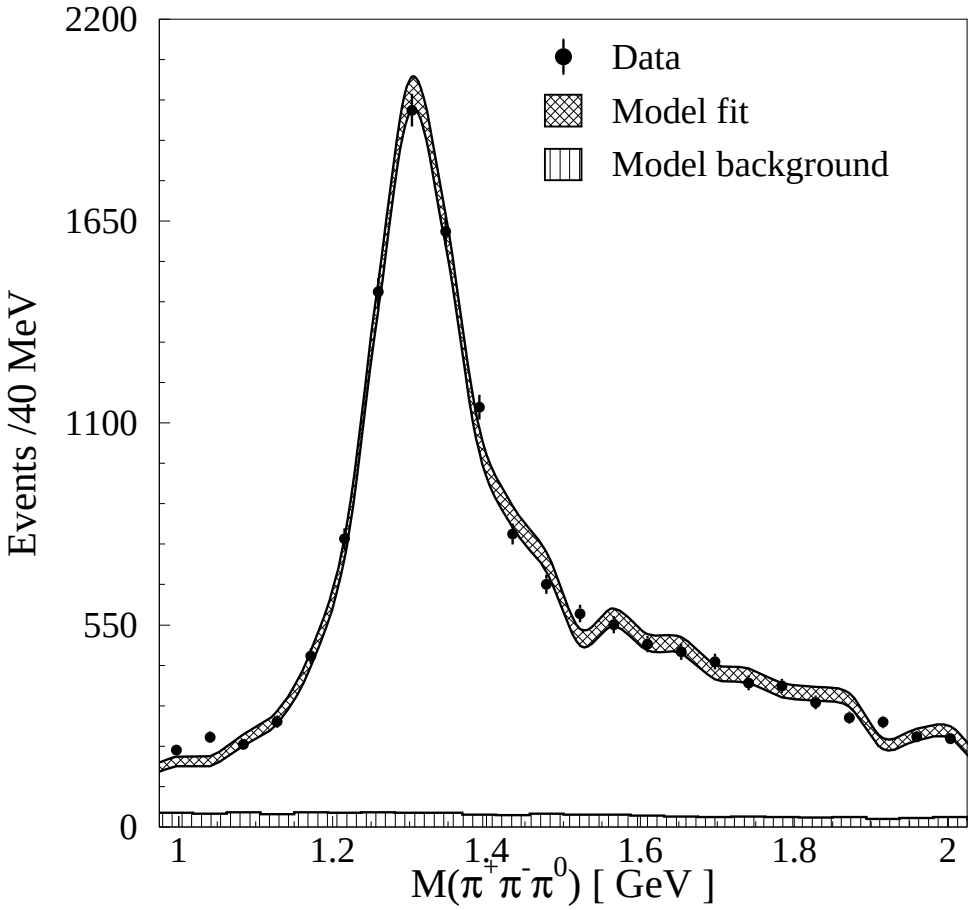


Figure 6: The $\pi^+\pi^-\pi^0$ mass distribution of the data (full points ) compared to the one obtained by the partial wave analysis fit ( fit curve with corridor of statitical errors) .

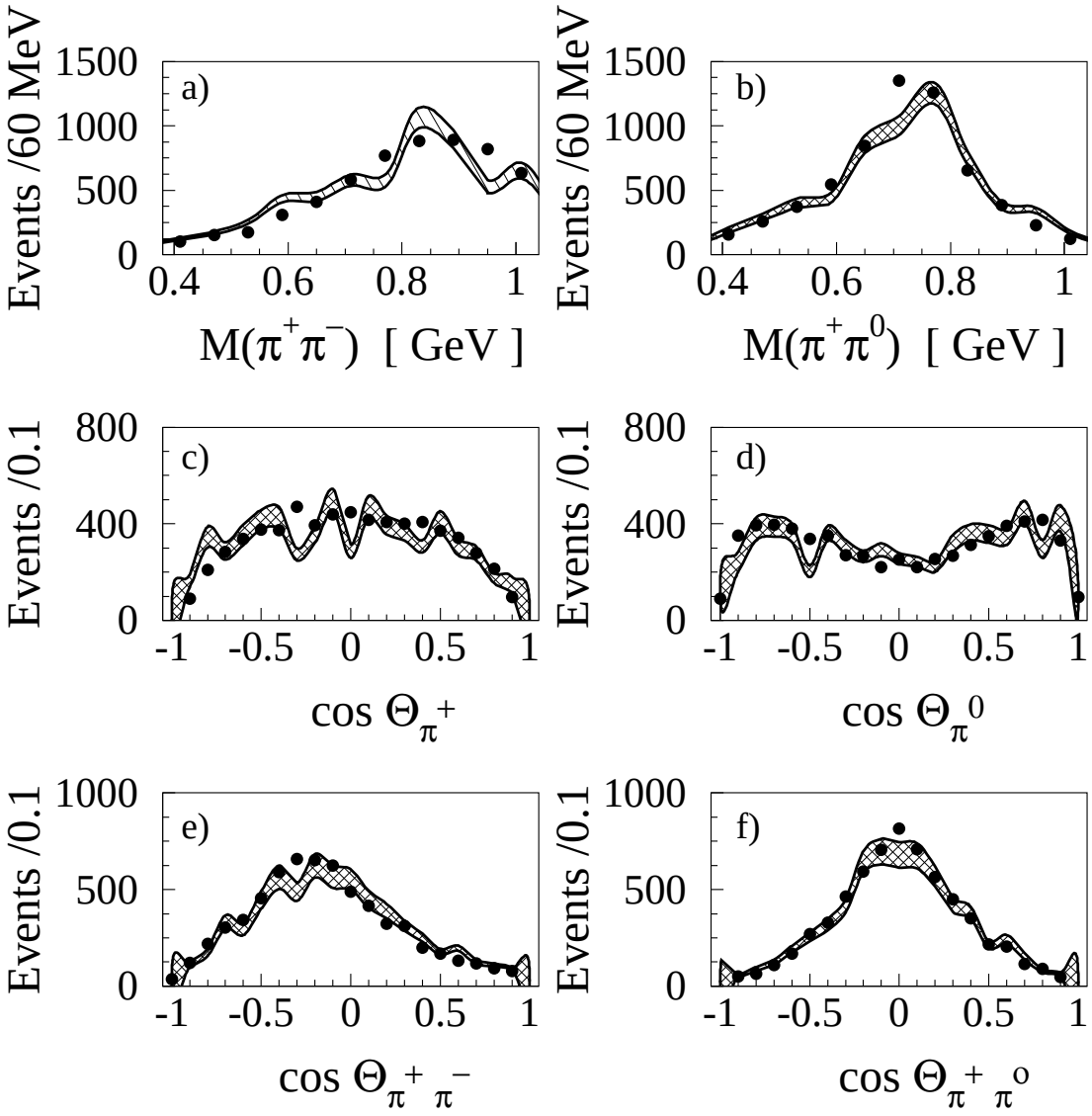


Figure 7: The description of mass and angular distributions for the two-photon energy slice 1200MeV $\leq$ $W_{\gamma\gamma}$ $\leq$ 1400MeV. a) The $\pi^+\pi^-$ mass projection, b) he $\pi^0\pi^\pm$ mass projection, c) the angular distribution of the charged pion in c.m.system of the reaction, d) the angular distribution of the neutral pion in c.m.system of the reaction, e) the angular distribution between positive and negative pions in $\pi^+\pi^0$ c.m.system, f) the angular distribution between neutral and negative pions in $\pi^+\pi^-$ c.m.system

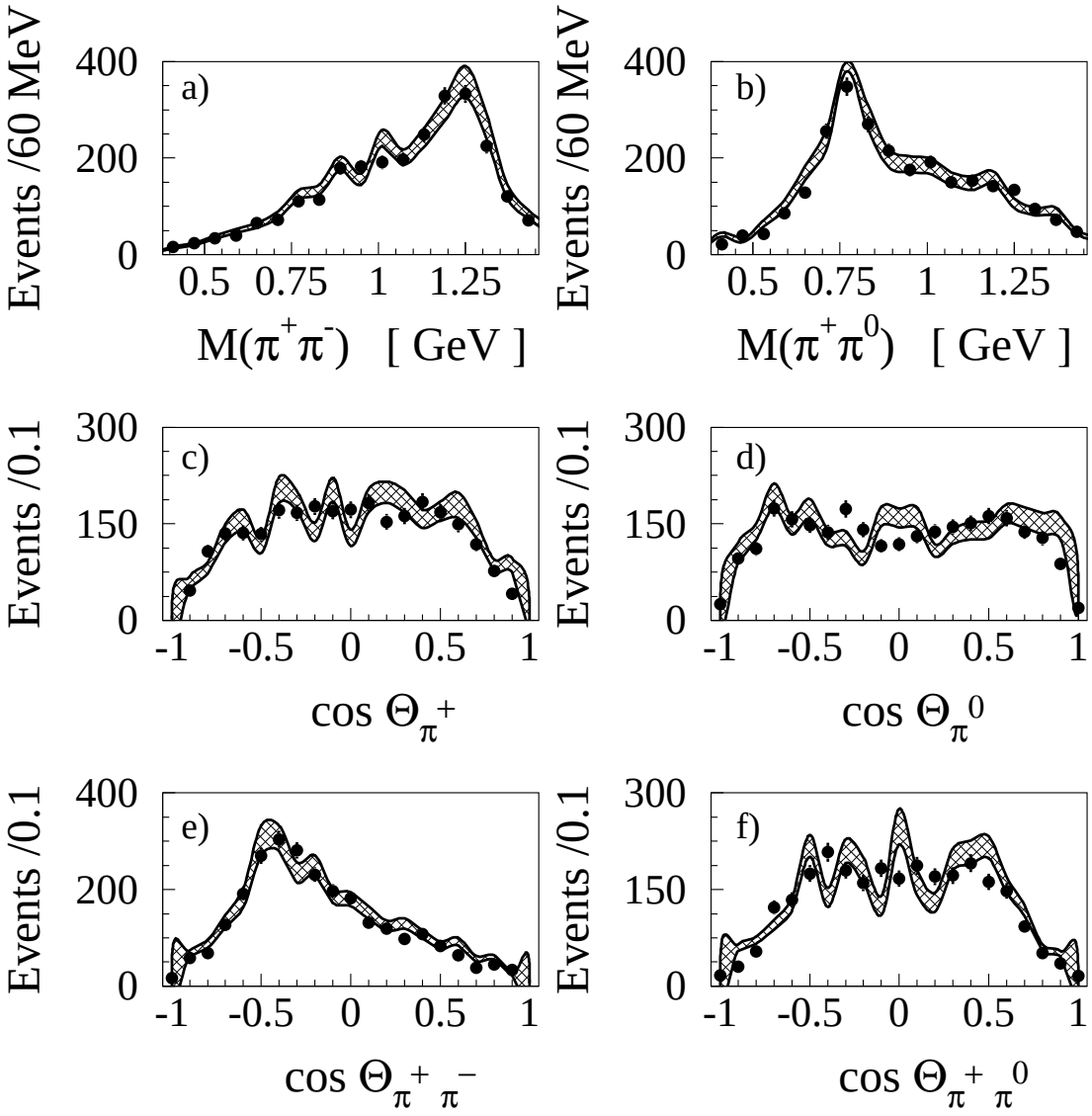


Figure 8: The description of mass and angular distributions for the two-photon energy slice 1600MeV $\leq$ $W_{\gamma\gamma}$ $\leq$ 1900MeV. a) The $\pi^+\pi^-$ mass projection, b) he $\pi^0\pi^\pm$ mass projection, c) the angular distribution of the charged pion in c.m.system of the reaction, d) the angular distribution of the neutral pion in c.m.system of the reaction, e) the angular distribution between positive and negative pions in $\pi^+\pi^0$ c.m.system, f) the angular distribution between neutral and negative pions in $\pi^+\pi^-$ c.m.system

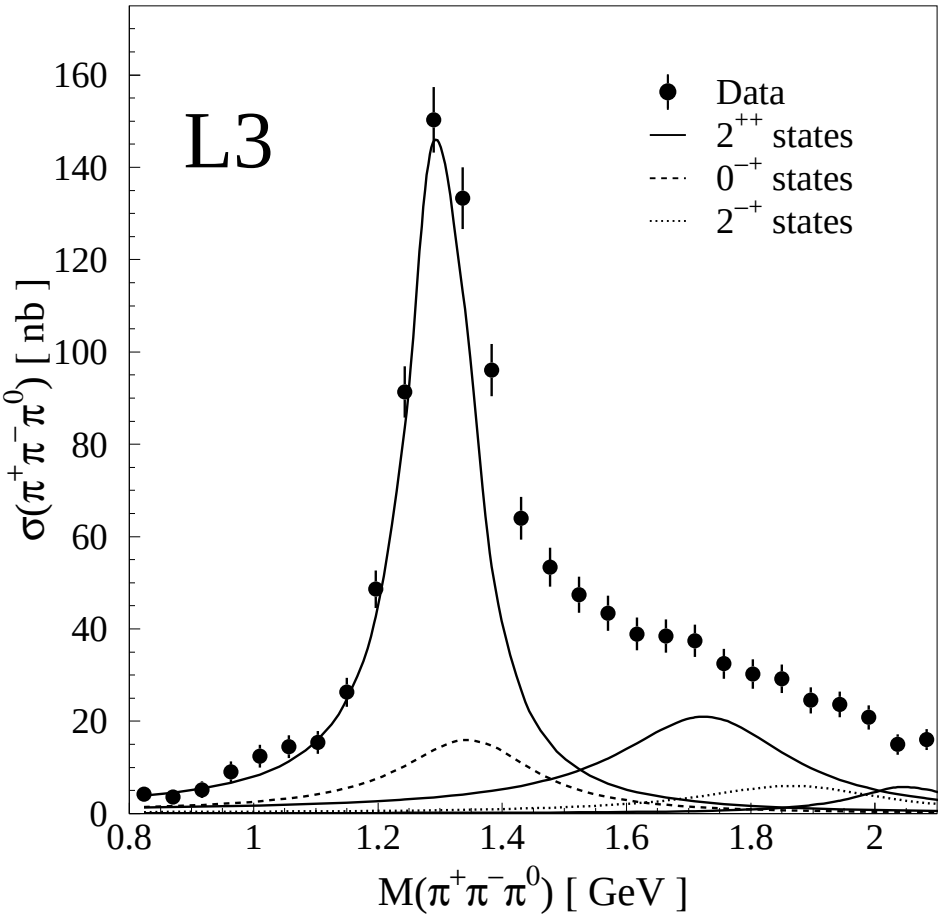


Figure 9: The contribution of the resonances to the cross section. The full cross section of $\gamma\gamma \to \pi^+\pi^-\pi^0$ reaction is calculated for $P_t < 0.1$ GeV cut and shown as points with error bars. The full curves correspond to three $2^{++}$ states, the dashed curve to the $0^{-+}$ and dotted curve to the $2^{-+}$ contributions.

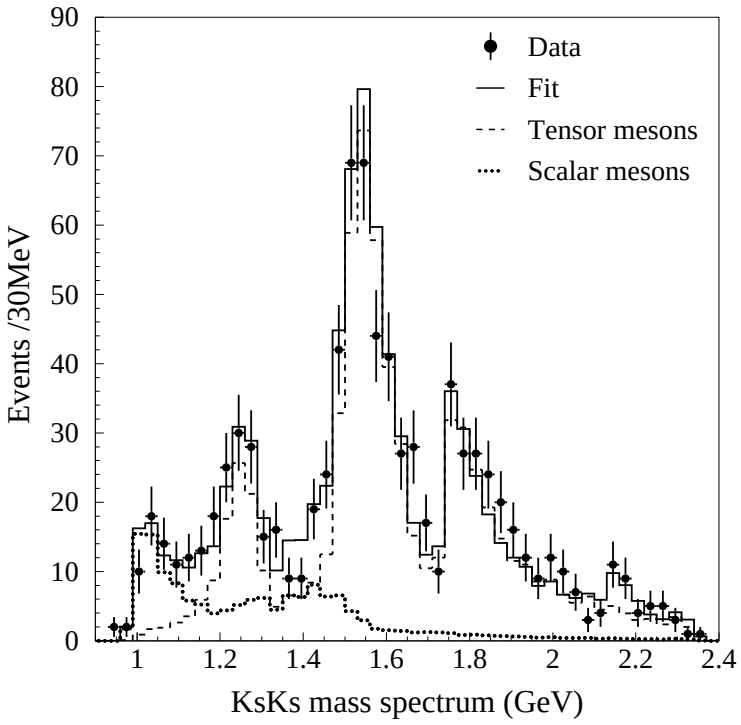


Figure 10: The description of the $\gamma\gamma$ spectrum for the $K_sK_s$ reaction. The data are show as points with errorbars, the solid curve corresponded to the fit with nonet relations imposed, dashed line shows the contribution of tensor states and dotted line the contribution of scalar states.

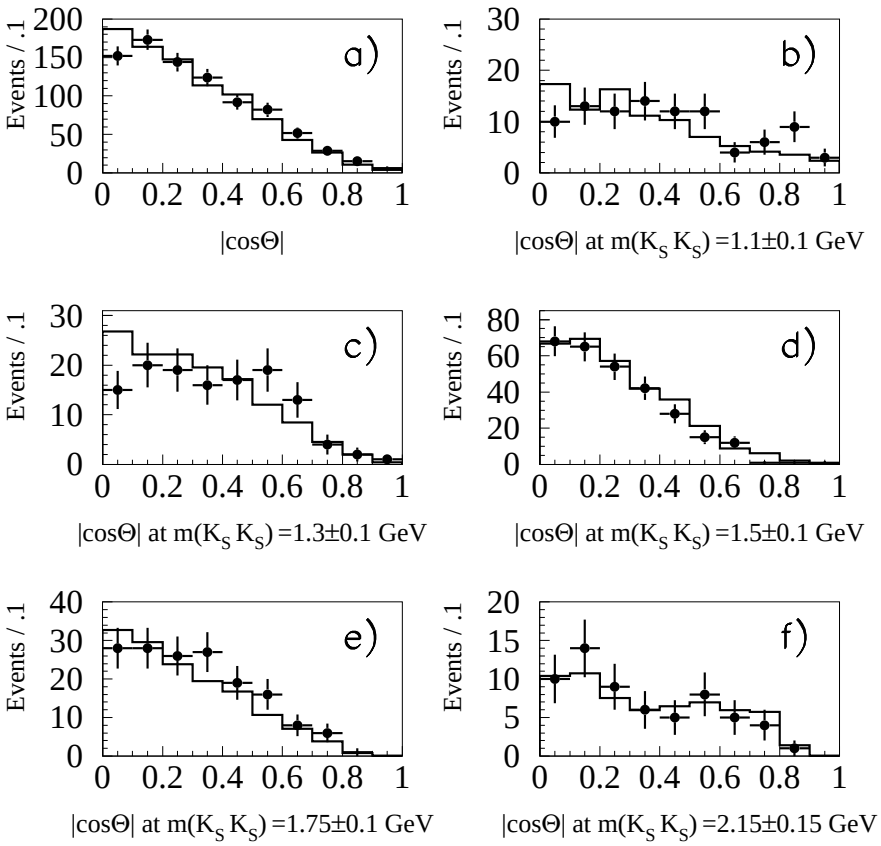


Figure 11: Description of angular distributions on $\gamma\gamma \to K_s K_s$ reaction. The data corresponds to points with errorbars, the description of the data (for the fit with nonet relations imposed) is shown by solid curves.

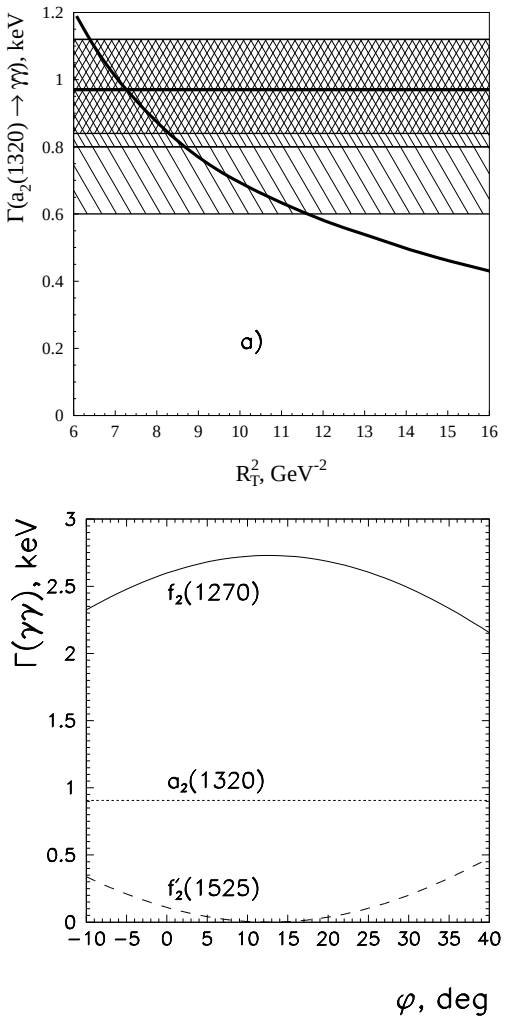


Figure 12: a) the dependence of $\gamma\gamma$ width of $a_2(1320)$ on radius of the state and b) the dependence of $\gamma\gamma$ widths of lowest isoscalar tensor mesons on mixing angle [11]

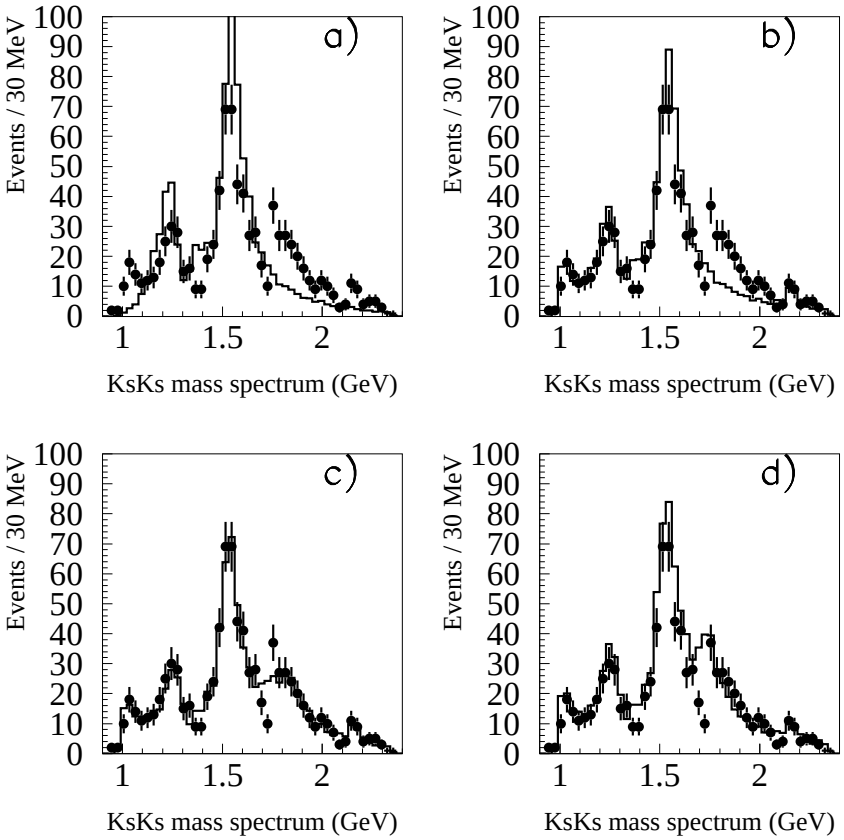


Figure 13: a) the description of the data with the first tensor nonet states only b) description of the data with the first tensor nonet, scalar states, $4^{++}$ states and nonresonant $2^{++}$ contribution. c) Fit of the data with components described in (b) and the $f_0(1710)$ state fitted with free parameters. d) same as (c) but mass and width of $f_0(1710)$ is fixed from latest BES results [15].

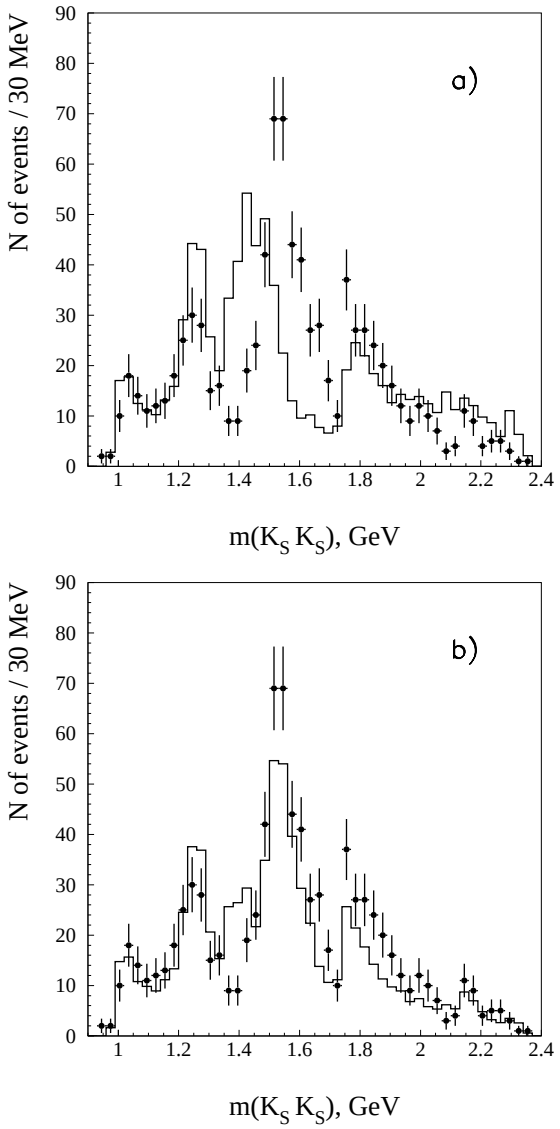


Figure 14: A description of the data with mixing angle of the first nonet fixed at a) 25 degrees and b) 7 degrees.